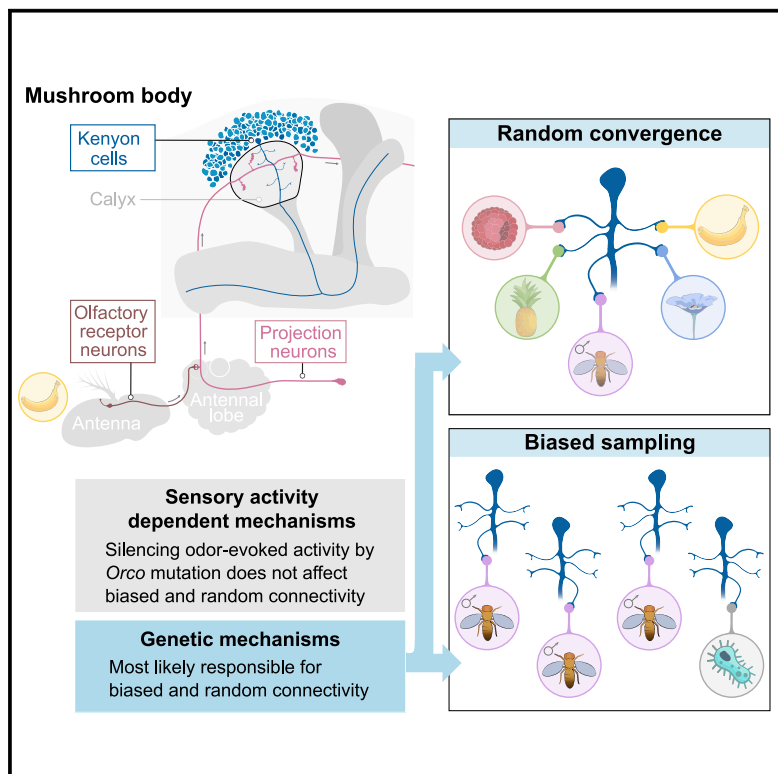


Mushroom body input connections form independently of sensory activity in *Drosophila melanogaster*

Graphical abstract



Authors

Tatsuya Tatz Hayashi,
Alexander John MacKenzie,
Ishani Ganguly, ...,
Miles Solomon Jacob,
Ashok Litwin-Kumar,
Sophie Jeanne Cécile Caron

Correspondence

sophie.caron@utah.edu

In brief

The connectivity architecture of higher brain centers can be regulated by genetic and activity-dependent mechanisms. Hayashi et al. test whether sensory activity is required to connect the Kenyon cells of *Drosophila melanogaster* mushroom body to the olfactory system and show that these connections form normally in the absence of sensory activity.

Highlights

- Kenyon cells in *Orco*^{-/-} flies show reduced responses to odors
- The connections between olfactory neurons and Kenyon cells form normally in *Orco*^{-/-}
- The input connections of Kenyon cells are genetically determined



Article

Mushroom body input connections form independently of sensory activity in *Drosophila melanogaster*

Tatsuya Tatz Hayashi,^{1,2} Alexander John MacKenzie,^{1,2} Ishani Ganguly,³ Kaitlyn Elizabeth Ellis,¹ Hayley Marie Smihula,¹ Miles Solomon Jacob,¹ Ashok Litwin-Kumar,³ and Sophie Jeanne Cécile Caron^{1,2,4,*}

¹School of Biological Sciences, University of Utah, Aline Skaggs Wilmot Biology Building, 257 South 1400 East, Salt Lake City, UT 84112, USA

²Neuroscience Program, University of Utah, Salt Lake City, UT 84112, USA

³Center for Theoretical Neuroscience, Columbia University, Jerome L Greene Science Center, 3227 Broadway, New York, NY 10027, USA

⁴Lead contact

*Correspondence: sophie.caron@utah.edu

<https://doi.org/10.1016/j.cub.2022.07.055>

SUMMARY

Associative brain centers, such as the insect mushroom body, need to represent sensory information in an efficient manner. In *Drosophila melanogaster*, the Kenyon cells of the mushroom body integrate inputs from a random set of olfactory projection neurons, but some projection neurons—namely those activated by a few ethologically meaningful odors—connect to Kenyon cells more frequently than others. This biased and random connectivity pattern is conceivably advantageous, as it enables the mushroom body to represent a large number of odors as unique activity patterns while prioritizing the representation of a few specific odors. How this connectivity pattern is established remains largely unknown. Here, we test whether the mechanisms patterning the connections between Kenyon cells and projection neurons depend on sensory activity or whether they are hardwired. We mapped a large number of mushroom body input connections in partially anosmic flies—flies lacking the obligate odorant co-receptor Orco—and in wild-type flies. Statistical analyses of these datasets reveal that the random and biased connectivity pattern observed between Kenyon cells and projection neurons forms normally in the absence of most olfactory sensory activity. This finding supports the idea that even comparatively subtle, population-level patterns of neuronal connectivity can be encoded by fixed genetic programs and are likely to be the result of evolved prioritization of ecologically and ethologically salient stimuli.

INTRODUCTION

The precise wiring between sensory systems and higher brain centers is orchestrated by a combination of hardwired and activity-dependent mechanisms.¹ Hardwired mechanisms include complex signaling networks that guide neuronal outgrowths to their target and cell surface molecules that pair synaptic partners. Such hardwired mechanisms are necessary to establish coarse connectivity patterns in a reproducible and reliable manner. In contrast, activity-dependent mechanisms—sensory or spontaneous activity—can refine these coarse patterns by promoting the connectivity of active inputs over that of inactive inputs. Although spontaneous activity can refine connectivity patterns independently of experience, sensory activity sculpts connections based on available information such that the overall structure of a network can be molded after the sensory environment peculiar to an organism.

The *Drosophila melanogaster* mushroom body is a higher brain center formed by 2,000 neurons called “Kenyon cells” and primarily processes olfactory information.^{2,3} The primary olfactory center in the fly brain, the antennal lobe, consists of 51 glomeruli; each glomerulus receives input from a set of

olfactory sensory neurons expressing the same receptor gene(s).^{4,5} Olfactory information is relayed from individual glomeruli to Kenyon cells by about 160 uniglomerular projection neurons.^{6,7} The connections between projection neurons and Kenyon cells are random: individual Kenyon cells integrate inputs from a small set of projection neurons that cannot be assigned to a common group based on their biological characteristics.^{3,8–10} Such a random connectivity pattern has been predicted by several theoretical studies to be advantageous, as it expands the capacity of the mushroom body to represent olfactory information by minimizing the overlap between representations.^{11,12}

Although random, the connections between projection neurons and Kenyon cells are also biased: not all projection neurons connect to Kenyon cells at the same frequency—some neurons are overrepresented, whereas others are underrepresented.^{3,9} Interestingly, the most biased projection neurons, both underrepresented and overrepresented neurons, receive input from olfactory sensory neurons narrowly tuned to detect odors that are particularly meaningful. For instance, the DP1m and DA1 projection neurons are among the most overrepresented neurons. The DP1m projection neuron receives input from the



IR64a-expressing olfactory sensory neurons, which detect acids produced by fermenting fruits, a potential food source, whereas the DA1 projection neurons receive input from the OR67d-expressing neurons, which detect the pheromone 11-cis-vaccenyl acetate.^{13,14} In contrast, underrepresented projection neurons are activated by odors that trigger strong innate avoidance, likely via mushroom-body-independent pathways. For instance, the DL4 and DA2 projection neurons are among the most underrepresented neurons. The DL4 projection neuron receives input from the OR49a/OR85f-expressing neurons that detect odors produced by parasitoid wasps, whereas the DA2 projection neurons receive input from the OR56a-expressing neurons that detect odors produced by toxic microbes.^{15,16}

Whether biases in connectivity arise through sensory activity—possibly through competitive interactions among projection neurons—or hardwired mechanisms is not known. To distinguish between these two possibilities, we sought to compare whether the mushroom body input connections differ between wild-type flies and flies in which most olfactory sensory neurons are silent.

RESULTS

Decreased odor-evoked activity in the mushroom body calyx of *Orco*^{-/-} flies

Orco—also known as OR83b—is the obligate co-receptor of all odorant receptors (ORs) in most insects.^{17,18} *Orco* is required for olfactory transduction, and, hence, OR-expressing neurons in *Orco*^{-/-} flies form normally but do not show odor-evoked responses.^{17,19,20} Of the 51 antennal lobe glomeruli, at least 37 receive input from OR-expressing sensory neurons (Table S1). The remaining glomeruli are innervated by olfactory sensory neurons expressing either ionotropic receptors (IRs), which are tuned to amines and acids, or gustatory receptors (GRs), which detect carbon dioxide.^{14,18,21,22} Both IRs and GRs do not require *Orco* as a co-receptor; therefore, *Orco*^{-/-} flies are not completely anosmic and can detect odors that bind to these receptors.^{14,23–26} To test whether these sensory defects are reflected in the mushroom body, we measured odor-evoked responses in the calyx—the neuropil where projection neurons connect with Kenyon cells—of 2- or 3-day-old female flies that express GCaMP6f in all Kenyon cells. As expected, we did not detect odor-evoked calcium transients in the calyx of *Orco*^{-/-} flies in response to the odors detected by ORs, but we detected odor-evoked responses to acetic acid, an odor detected by IRs (Figures 1 and S1). In contrast, the calyx of *Orco*^{+/+} flies show large calcium transients in response to all odors.

These results show that sensory activity is severely impaired in the mushroom body of *Orco*^{-/-} flies: although Kenyon cells can respond an odor detected by IR-expressing neurons, they fail to respond to odors detected by OR-expressing neurons.

Glomeruli of the antennal lobe are morphologically similar in *Orco*^{+/+} and *Orco*^{-/-} flies

Next, we investigated whether the neuroanatomy of the antennal lobe of *Orco*^{-/-} flies differs from that of *Orco*^{+/+} flies. Previous studies have demonstrated that in *Orco*^{-/-} flies olfactory sensory neurons are able to target their cognate glomeruli.^{20,24,27}

However, a recent study showed that in ants, *Orco* loss of function leads to smaller antennal lobes that contain fewer glomeruli.^{28,29} To verify whether similar defects are found in *Orco*^{-/-} flies, we reconstructed their antennal lobes and identified individual glomeruli based on available anatomical maps as well as the hemibrain connectome.^{4,5,30} We identified a total of 51 glomeruli in both genotypes (Figure 2A). The total volume of individual antennal lobes in *Orco*^{+/+} and *Orco*^{-/-} flies is not significantly different (antennal lobe volume [median]: *Orco*^{+/+}, 84,723 μm^3 [n = 5]; *Orco*^{-/-}, 81,128 μm^3 [n = 5], p = 0.15; Figure 2B; Table S1). However, some glomeruli receiving input from OR-expressing neurons are slightly but significantly smaller in *Orco*^{-/-} flies, whereas some glomeruli receiving input from IR/GR-expressing neurons are slightly but significantly larger (Figure 2C; Table S1). These results support the previous finding suggesting that glomerular volume is subject to activity-dependent mechanisms.^{31–33}

Altogether, these results show that the antennal lobes form mostly normally in the absence of sensory activity: all glomeruli are formed in *Orco*^{-/-} flies, but a few of them vary in size when compared with *Orco*^{+/+} glomeruli.

Projection neurons and Kenyon cells are morphologically similar in *Orco*^{+/+} and *Orco*^{-/-} flies

Next, we investigated whether the projection neurons connecting individual glomeruli to Kenyon cells show morphological differences between *Orco*^{+/+} and *Orco*^{-/-} flies. To this end, we photo-labeled the neurons innervating different glomeruli: the DL4 glomerulus, which receives input from the OR49a+/OR85f+ neurons; the DM2 glomerulus, which receives input from the OR22a+ neurons; the DM5 glomerulus, which receives input from the OR85a+ neurons; the VA2 glomerulus, which receives input from the OR92a+ neurons; and the DP1m glomerulus, which receives input from the IR64a+ neurons (Figures 3A and S2A). For each glomerulus, we recovered the expected number of photo-labeled projection neurons in both genotypes (Figures 3B and S2B). We quantified the number of primary branches these neurons extend in the mushroom body calyx, their total and average length, and the number of forks they form (Figures 3C–F, S2C, and S2D); we also measured the volume of the presynaptic sites—or “boutons”—formed by a given type of projection neuron (Figures 3G and S2E; Videos S1 and S2). Based on these measurements, we found that the projection neurons of *Orco*^{+/+} and *Orco*^{-/-} flies are largely comparable. There are some small but significant differences: the DL4 projection neurons form fewer and shorter primary branches in *Orco*^{-/-} flies (number of branches [median]: *Orco*^{+/+}, 3 [n = 10]; *Orco*^{-/-}, 2 [n = 10], p = 0.02; total branch length (median): *Orco*^{+/+}, 27.1 μm [n = 10]; *Orco*^{-/-}, 18.1 μm [n = 10], p = 0.01); the VA2 projection neurons form longer branches in *Orco*^{-/-} flies (total branch length [median]: *Orco*^{+/+}, 137.4 μm [n = 10]; *Orco*^{-/-}, 193.0 μm [n = 10], p = 0.0003), and the volume of the boutons formed by the VA2 projection neurons is slightly larger in *Orco*^{-/-} flies (bouton volume [median]: *Orco*^{+/+}, 422.8 μm^3 [n = 10]; *Orco*^{-/-}, 602.3 μm^3 [n = 10], p = 0.03; Figures 3B–3G).

Next, we determined whether Kenyon cells show morphological differences between *Orco*^{+/+} and *Orco*^{-/-} flies. Based on their axonal projection patterns, Kenyon cells can be divided into three major types: α/β , α'/β' , and γ Kenyon cells.² It has

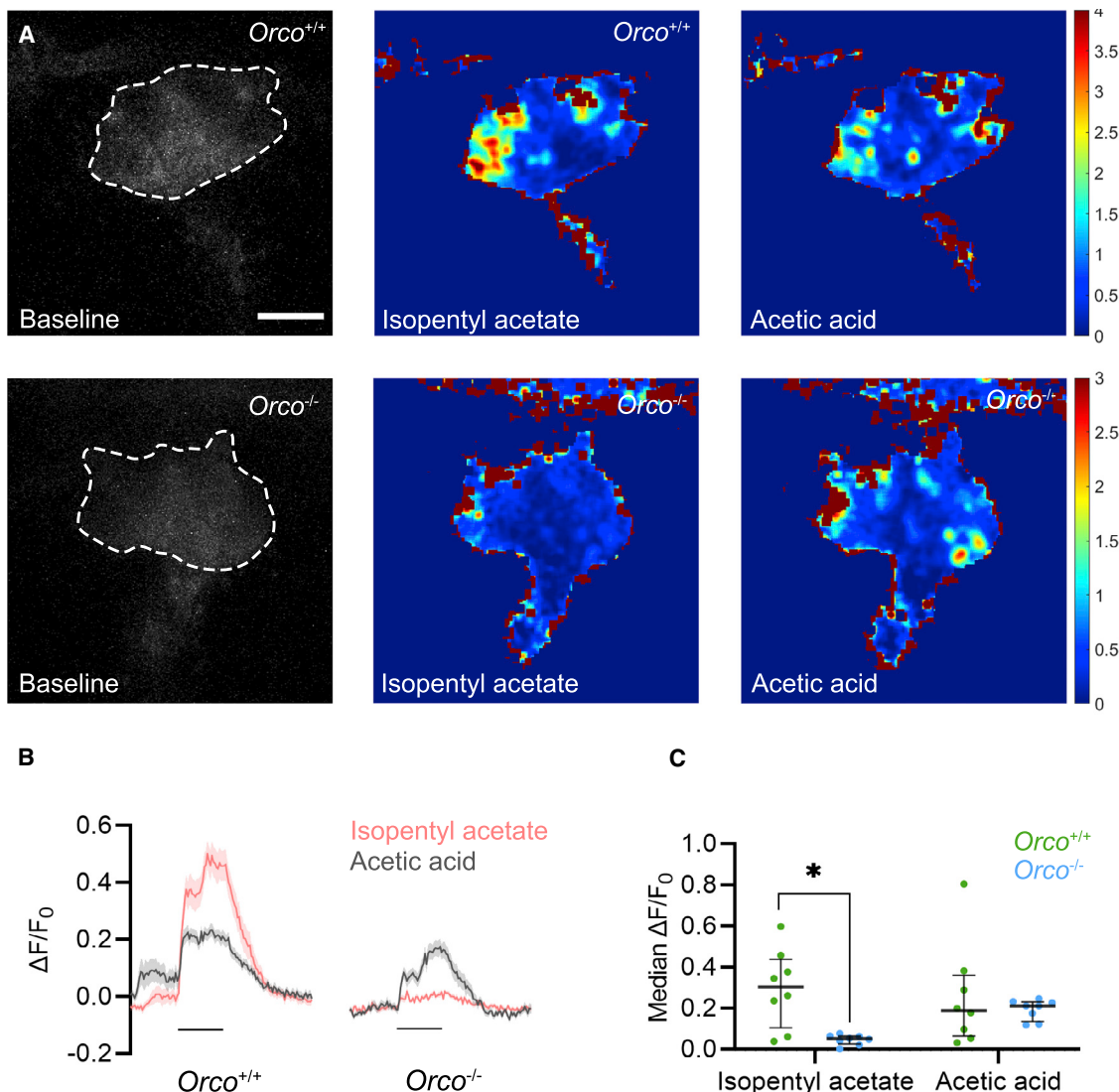


Figure 1. Odor-evoked activity is decreased in the mushroom body calyx of *Orco*^{-/-} flies

(A–C) Calcium imaging in Kenyon cells shows odor-evoked activity in *Orco*^{-/-} flies in response to isopentyl acetate, an odor that activates multiple odorant receptors, but not in response to acetic acid, an odor that activates ionotropic receptors.

(A) The calcium indicator GCaMP6f was expressed in all Kenyon cells using the *R13F02* transgene. Guided by baseline fluorescence, the region where Kenyon cells extend their dendrites—the calyx of the mushroom body—was identified in *Orco*^{+/+} and *Orco*^{-/-} female flies that are 2 or 3 days old (left column, dashed white line). Example heatmaps show $\Delta F/F_0$ in response to isopentyl acetate (middle column) and acetic acid (right column). The color bars denote the range of $\Delta F/F_0$ in each sample. Scale bars, 20 μ m.

(B) The $\Delta F/F_0$ values recorded in the main calyx in response to isopentyl acetate (pink) and acetic acid (gray) were averaged across eight trials collected in eight different animals and are shown as traces; the shaded area of each trace represents the SEM.

(C) The median $\Delta F/F_0$ values during odor presentation were averaged across trials in *Orco*^{+/+} (green) and *Orco*^{-/-} (blue) flies ($n = 8$); the long black bars represent the median, whereas the short black bars represent the 25th and 75th percentile of the data.

The statistical significance was measured using the Mann-Whitney U test; the asterisk indicates values that were statistically different ($p < 0.05$). See also Figure S1.

previously been shown that the number of post-synaptic terminals, or “claws,” formed by a neuron varies across types.^{3,9} We photo-labeled individual Kenyon cells of each type and compared their morphological features between *Orco*^{+/+} and *Orco*^{-/-} genotypes (Figures 4A and S3). Specifically, we measured the total and average length of the branches individual Kenyon cells extend in the calyx, as well as the number and

length of the claws formed by these neurons (Figures 4B–4E and S3). We detected one significant difference: γ Kenyon cells form longer branches in *Orco*^{-/-} flies than they do in *Orco*^{+/+} flies (total branch length [median]: *Orco*^{+/+}, 87.8; *Orco*^{-/-}, 147.0, $p = 0.02$ [$n = 10$]; Figure 4B). It is possible that the observed morphological differences in the γ Kenyon cells of *Orco*^{-/-} flies result from activity-dependent pruning mechanisms as described in a

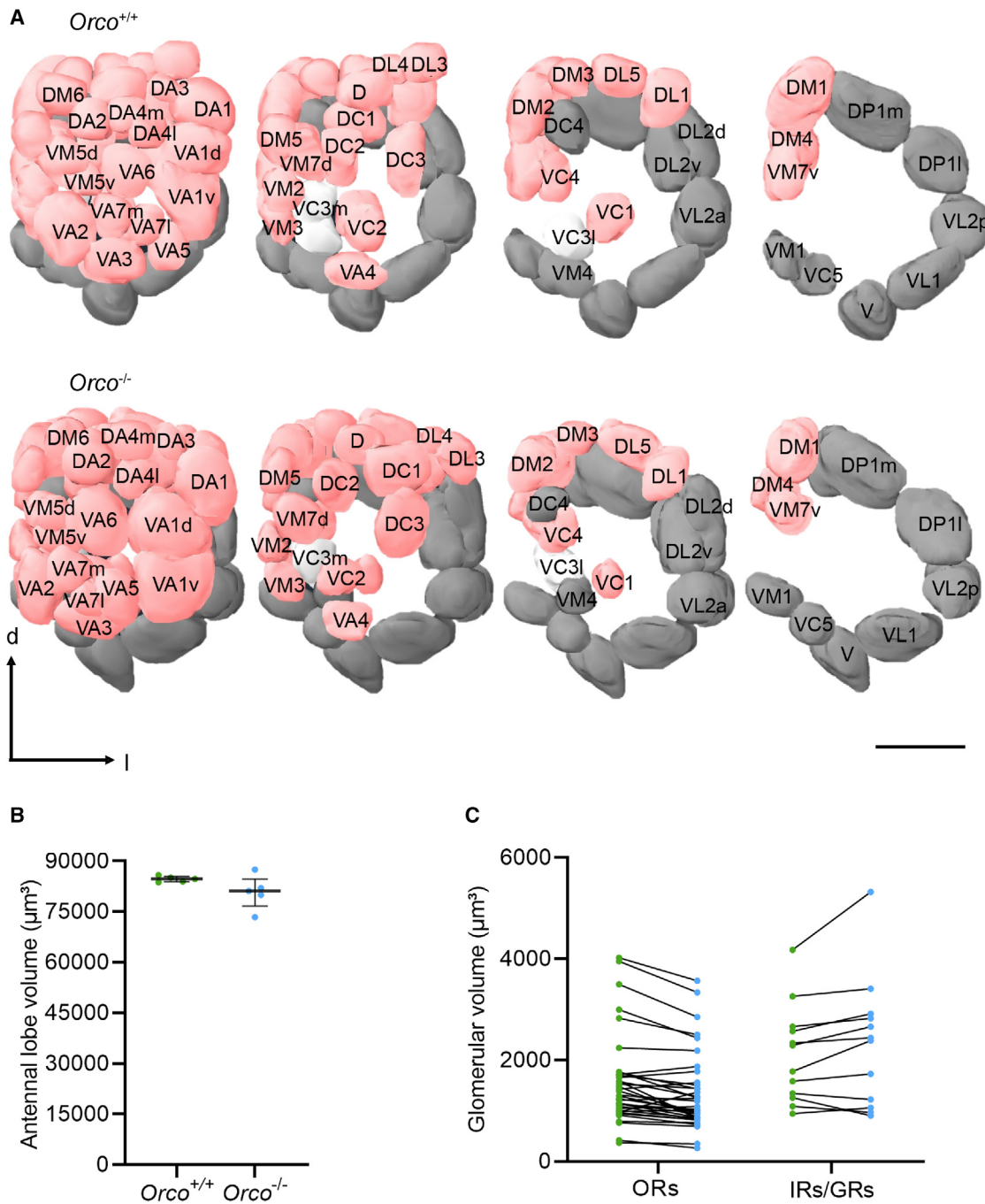


Figure 2. Antennal lobes are morphologically similar in *Orco^{+/+}* and *Orco^{-/-}* flies

(A) The brains of 2- or 3-day-old *Orco^{+/+}* and *Orco^{-/-}* female flies were fixed, immuno-stained (using the nc82 monoclonal antibody against Bruchpilot) and imaged; each of the 51 glomeruli forming the antennal lobe were reconstructed and identified based on their shapes and locations; each glomerulus receives input from either OR-expressing neurons (pink), IR/GR-expressing neurons (dark gray), or unidentified receptor neurons (light gray). Scale bars, 25 μm .

(B and C) The reconstructed volumes of the entire antennal lobe (B) or individual glomeruli (C) were compared across genotypes (green, *Orco^{+/+}* [n = 5]; blue, *Orco^{-/-}* [n = 5]); the long black bars represent the median, whereas the short black bars represent the 25th and 75th percentile of the data.

(C) The volumes of a given glomerulus in both genotypes are linked with a black line.

The statistical significance was measured using the Mann-Whitney U test; the statistical significance of the differences in glomerular volumes is provided in Table S1.

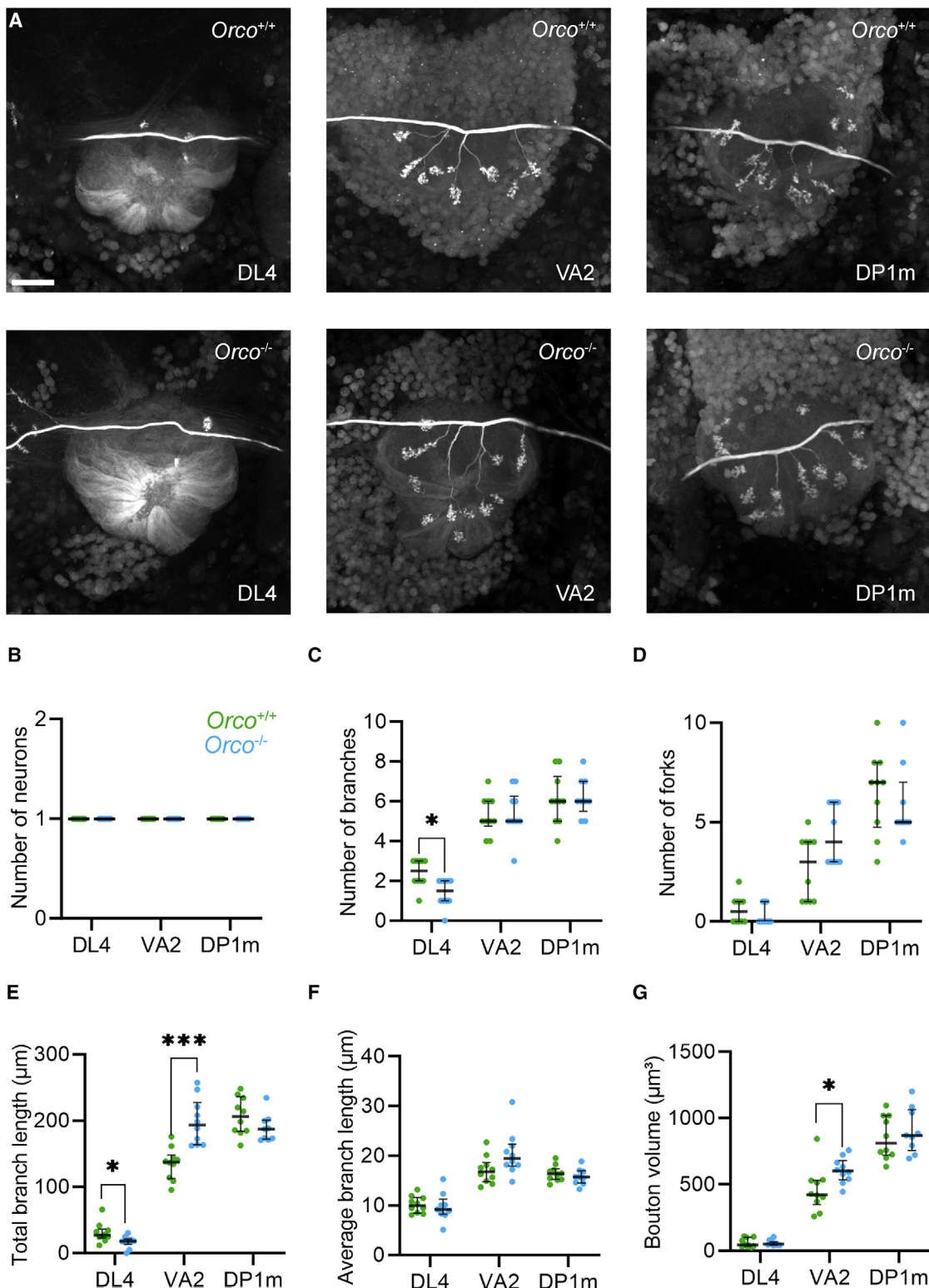


Figure 3. Projection neurons are morphologically similar in *Orco^{+/+}* and *Orco^{-/-}* flies

(A) The projection neurons innervating the DL4 (left), VA2 (middle), and DP1m (right) glomeruli were photo-labeled in *Orco^{+/+}* and *Orco^{-/-}* female flies that were 2 or 3 days old, and the presynaptic terminals—called “boutons”—formed by these neurons in the calyx of the mushroom body were imaged. Scale bars, 15 μm .

(legend continued on next page)

recent study.³⁴ However, apart from this subtle difference, Kenyon cells are morphologically similar in both genotypes. Most importantly, Kenyon cells form the same number of claws—and therefore receive the same number of inputs—in *Orco*^{+/+} and *Orco*^{-/-} flies (Figure 4D).

Altogether, these results suggest that both projection neurons and Kenyon cells formed in *Orco*^{-/-} flies show no obvious morphological defects.

Mushroom body input connections in *Orco*^{-/-} flies are biased and random

If sensory activity affects the way projection neurons connect to Kenyon cells, we would expect these connections to be qualitatively and quantitatively different in *Orco*^{+/+} and *Orco*^{-/-} flies. To compare global and more subtle connectivity patterns between genotypes, we used a neuronal tracing technique we previously devised.⁹ In short, individual Kenyon cells were photo-labeled, and their input projection neurons were identified using dye electroporation. With this technique, the inputs of hundreds of Kenyon cells can be identified and reported in a connectivity matrix. Statistical analyses of the resulting matrix can be used to reveal patterns of connectivity, including randomness and biases. We generated two connectivity matrices using *Orco*^{+/+} and *Orco*^{-/-} flies—henceforth referred to as the “*Orco*^{+/+} matrix” and the “*Orco*^{-/-} matrix”—by mapping the inputs of 250 Kenyon cells in each genotype; each matrix contains 887 and 899 connections, respectively (Figure 5A).

We used different statistical analyses to compare these matrices. As a first step, we measured the frequencies at which projection neurons connect to Kenyon cells (Figures 5B and 5C; Table S2). Lack of sensory activity could affect the frequencies at which projection neurons connect to Kenyon cells in at least two different ways. First, it is conceivable that the number of connections formed by projection neurons receiving input from OR-expressing neurons would be higher in *Orco*^{+/+} flies, where they receive functional input, than in *Orco*^{-/-} flies, where their input neurons are silent. Such differences would be especially noticeable for projection neurons that connect to Kenyon cells at high frequencies in *Orco*^{+/+} flies, such as the DA1 projection neurons. However, we could not detect such differences: all projection neurons that receive input from ORs-expressing neurons—including the DA1 projection neurons—connect at similar frequencies in both genotypes (DA1 connectivity frequencies: *Orco*^{+/+}, 3.38%; *Orco*^{-/-}, 3.11%, p = 0.89; Figure 6A; Table S2). Second, it is possible that the number of connections formed by projection neurons receiving input from IR/GR-expressing neurons would be higher in *Orco*^{-/-} flies, where they are the only neurons that receive functional input, than in *Orco*^{+/+} flies. This would support the idea that projection neurons compete when connecting with Kenyon cells and that projection neurons that receive active input are advantaged. Such differences would be especially noticeable for projection neurons

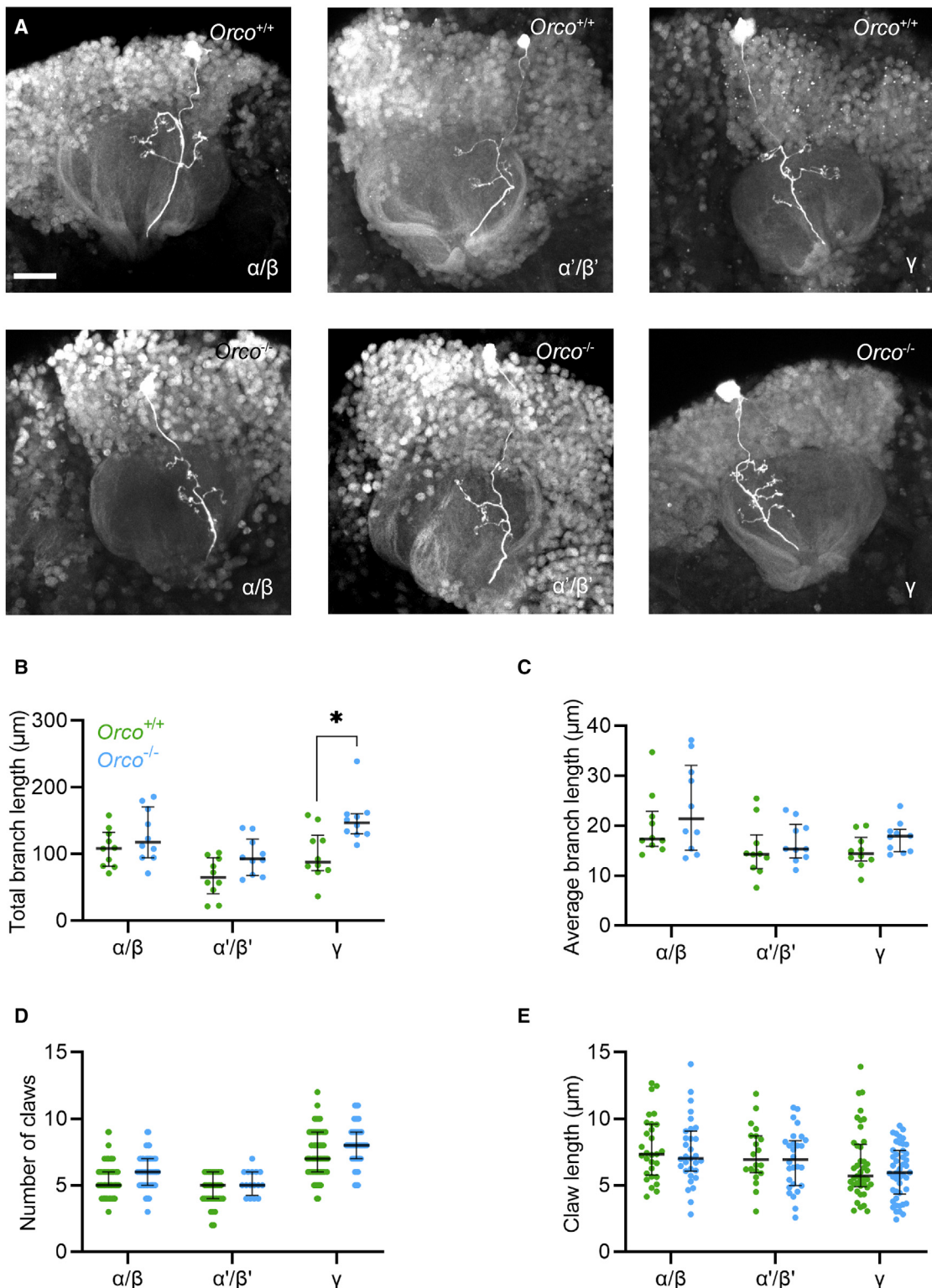
that connect to Kenyon cells at low frequencies in *Orco*^{+/+} flies, such as the VL1 projection neurons, as well as for projection neurons that connect at high frequencies, such as the DP1m neuron. However, we could not detect such differences: all projection neurons that receive input from IR/GR-expressing neurons—including the VL1 and DP1m projection neurons—connect at similar frequencies in both genotypes (VL1 connectivity frequencies: *Orco*^{+/+}, 0.56%; *Orco*^{-/-}, 0.33%, p = 0.72; DP1m: *Orco*^{+/+}, 5.07%; *Orco*^{-/-}, 3.67%, p = 0.17; Figure 6A; Table S2). We could not detect shifts in connectivity frequencies that were significant; the most significant shift detected was for the VL2a projection neurons (VL2a connectivity frequencies: *Orco*^{+/+}, 1.58%; *Orco*^{-/-}, 2.67%, p = 0.13; Figure 6A; Table S2). The connectivity frequencies measured for each projection neuron are largely similar across Kenyon cell types in both genotypes (Figures 6B–6D; Tables S3–S5). These frequencies are comparable with those measured in the hemibrain connectome, but we also observed some discrepancies (Figure 6; Table S2).³ These discrepancies are most likely due to the different methods used to map and score connections (STAR Methods).

As a second step, we used the Jensen-Shannon distance—a statistical method that measures the likeness of two probability distributions—as a global readout of similarity in the observed connectivity biases. A distance of 0 would indicate that the two probability distributions are identical, whereas larger distances would indicate that the two probability distributions are different. To gauge the extent to which the Jensen-Shannon distance indicates likeness in our datasets, we generated two different shuffled versions of the connectivity matrices. In one version, called “shuffle,” the connections between projection neurons and Kenyon cells were randomly shuffled by choosing input projection neurons without replacement while keeping the number of Kenyon cells and number of projection neuron inputs to each Kenyon cell consistent with the experimental matrices. In the other version, called “fixed-shuffle,” the connections were randomly shuffled, but the frequencies at which projection neurons connect to Kenyon cells were fixed to reflect the frequencies measured experimentally. When we compared the *Orco*^{+/+} and *Orco*^{-/-} matrices with their shuffled versions, we obtained distances ranging from 0.227 to 0.266; when we compared the experimental matrices with their fixed-shuffle versions, we obtained distances ranging from 0.087 to 0.149 (Figure 7A). The Jensen-Shannon distance measured when comparing the *Orco*^{+/+} and *Orco*^{-/-} matrices is 0.115—a value in the range of the values obtained with the fixed-shuffle matrices but outside the range of the values obtained with the shuffle matrices—suggesting that the distribution of connectivity frequencies is largely similar in both genotypes.

As a final step, we used an unbiased search for structural patterns that might exist in the connectivity matrices and that are not detectable by simply examining connectivity frequencies. To this

(B–G) The number of neurons photo-labeled (B), the number of primary branches (C) and forks (D) formed by the photo-labeled neurons, and the total and average branch length (E and F) were quantified in *Orco*^{+/+} (green; DL4, n = 10; VA2, n = 10; DP1m, n = 10) and *Orco*^{-/-} flies (blue; DL4, n = 10; VA2, n = 10; DP1m, n = 9); the total bouton volume was quantified (G). The long black bars represent the median, whereas the short black bars represent the 25th and 75th percentile of the data.

The statistical significance was measured using the Mann-Whitney U test; the asterisks indicate values that were statistically different (*p < 0.05 and **p < 0.01). See also Figure S2.

**Figure 4. Kenyon cells are morphologically similar in *Orco^{+/+}* and *Orco^{-/-}* flies**

(A) Individual α/β (left), α'/β' (middle), and γ Kenyon cells (right) were photo-labeled in *Orco^{+/+}* (top) and *Orco^{-/-}* (bottom) female flies that were 2 or 3 days old, and the post-synaptic terminals formed by these neurons in the mushroom body calyx—called “claws”—were imaged. Scale bars, 15 μm .

(legend continued on next page)

end, we extracted correlations within each connectivity matrix—experimental and fixed-shuffle matrices—using principal component analysis (Figure 7B). The percent variance associated with the different principal component projections provides a sensitive measure of structure within each matrix.⁹ For all components, the percent variance measured for the experimental matrix falls within the range measured for the fixed-shuffle matrices, suggesting that there are no structural patterns in the *Orco*^{+/+} and *Orco*^{-/-} matrices other than the biases in connectivity frequencies. It is worth noting that a recent study identified in a *Drosophila* connectome a group of projection neurons that appear to preferentially connect to the same Kenyon cells, but we could not find evidence for such group structure in our datasets (Figure S4).³⁵

Altogether, these results show that the mechanisms underlying the biased and random connectivity pattern observed among the mushroom body input connections does not depend on sensory activity and is therefore most likely hardwired.

DISCUSSION

In this study, we investigated whether the biased and random connectivity pattern observed between projection neurons and Kenyon cells forms depending on available sensory information. We first showed that in *Orco*^{-/-} flies, Kenyon cells fail to respond to odors detected by ORs but respond normally to odors detected by IRs. Second, we showed that—despite being partially anosmic—*Orco*^{-/-} flies develop a largely normal olfactory circuit: all glomeruli forming the antennal lobe can be identified in *Orco*^{-/-} flies, and the projection neurons and Kenyon cells found in *Orco*^{-/-} flies are morphologically similar to those found in *Orco*^{+/+} flies. Third, we mapped a large number of connections between projection neurons and Kenyon cells in *Orco*^{+/+} and *Orco*^{-/-} flies and compared the observed connectivity patterns using various statistical analyses. We could not detect any significant differences: projection neurons connect with Kenyon cells at similar frequencies in both datasets. Altogether, these results suggest that the biased and random connectivity pattern observed between projection neurons and Kenyon cells forms independently of sensory activity.

It is possible that there are subtle connectivity patterns established by sensory activity that have eluded our analyses. For instance, a previous study identified a small number of α/β and α'/β' Kenyon cells that receive input more frequently from a group of ten glomeruli tuned to different food odors.³⁵ However, we failed to detect similar group structure in both the *Orco*^{+/+} and *Orco*^{-/-} connectivity matrices, suggesting that our mapping strategy cannot be used to reveal such subtle connectivity patterns. More exhaustive mapping strategies—such as the derivation of an *Orco*^{-/-} connectome—might be necessary to determine whether this possible group structure might result from sensory activity. However, our technique is clearly able to detect global, population-level connectivity

patterns, and our results show that these patterns form independently of sensory activity.

This independence of sensory activity came as a surprise in light of the evidence, suggesting that the synapse between projection neurons and Kenyon cells is plastic in *Drosophila melanogaster*. Previous study noticed that when a few projection neurons are silenced or chronically activated, the volumes of their presynaptic terminals change in the mushroom body as well as the magnitudes of odor-evoked calcium transients.^{36–38} Another study showed that appetitive conditioning leads to an increase in the number of synapses formed between the projection neurons activated by the conditioned odor and Kenyon cells;³⁹ similar observations have been made in honeybees.⁴⁰ However, none of these studies could determine whether these plastic changes lead to lasting changes in connectivity pattern. Our results partially support these findings: we found that lack of sensory activity affects the morphology of the presynaptic terminals formed by some projection neurons in the mushroom body. However, our results also demonstrate that these sensory-based changes have no effect on the global connectivity pattern between projection neurons and Kenyon cells.

Our results support the idea that the biased and random connectivity pattern observed between projection neurons and Kenyon cells results from hardwired mechanisms. It is possible that such mechanisms regulate spontaneous activity either at the level of olfactory sensory neurons or at the level of projection neurons. This possibility appears, however, unlikely considering that olfactory sensory neurons in *Orco*^{-/-} flies show drastically reduced levels of spontaneous activity.¹⁷ Likewise, a previous study showed the DL1 and VM2 projection neurons in flies lacking their cognate receptor genes—*OR10a*^{-/-} and *OR43b*^{-/-} flies, respectively—are virtually silent and display low to no spontaneous activity.²⁴ Thus, the hardwired mechanisms leading to biases in connectivity most likely involve synapse-promoting factors which may be differentially expressed in overrepresented versus underrepresented neurons. A recent study found that the number of Kenyon cells affects the number of presynaptic sites formed by projection neurons: the more Kenyon cells there are, the fewer presynaptic sites.⁴¹ This result suggests that Kenyon cells might release a synapse-promoting signal that is differentially detected by projection neurons leading to the observed connectivity biases.

In theory, biased and random input connections are connectivity patterns that antagonize each other: the lack of structure afforded by randomization of inputs enables the mushroom body to represent olfactory information with as many unique activity patterns as possible, whereas the structure imposed by biases skews these representations to prioritize a few ethologically meaningful odors. Our finding that biases do not simply reflect the concrete chemosensory ecology of a fly but are hardwired suggests that this connectivity pattern has been shaped on a long-term evolutionary timescale. It is tempting to speculate that biases might prepare the mushroom body to learn more

(B–E) The total and average branch length formed by a Kenyon cell was measured (B and C), the number of claws formed by a Kenyon cell was counted (D), and the average length of a claw was measured (E) in *Orco*^{+/+} (green) and *Orco*^{-/-} flies (blue). The long black bars represent the median, whereas the short black bars represent the 25th and 75th percentile of the data.

The statistical significance was measured using the Mann-Whitney U test; the asterisk indicates values that were statistically different ($p < 0.05$). See also Figure S3.

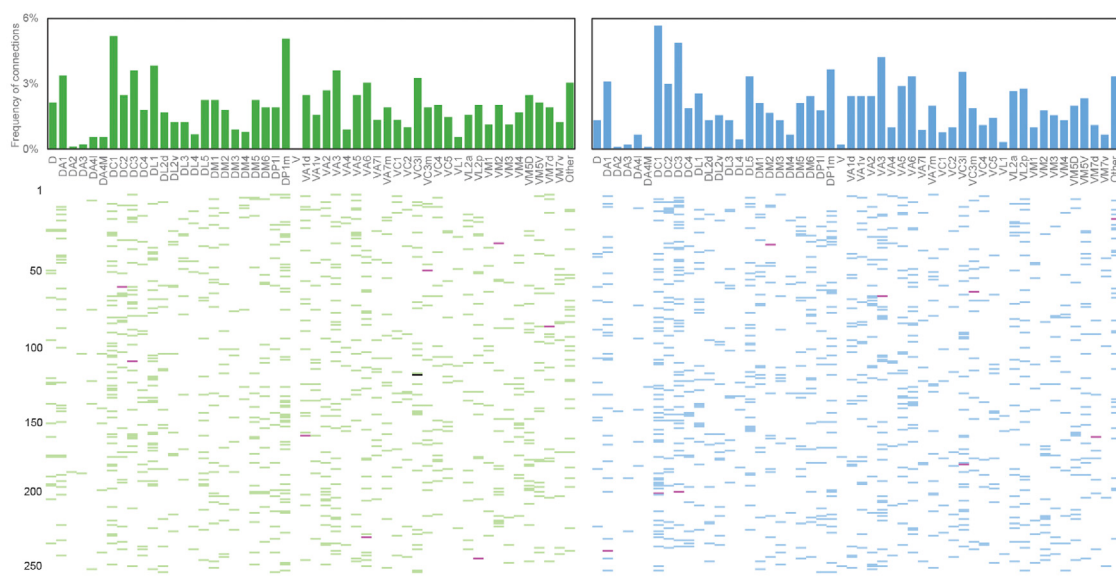
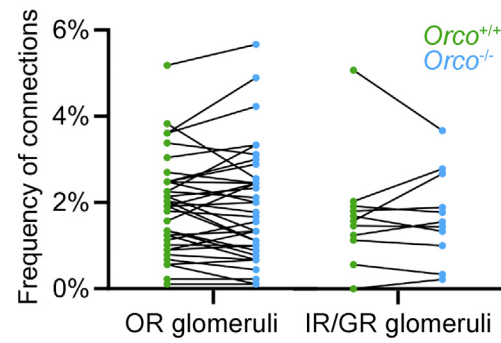
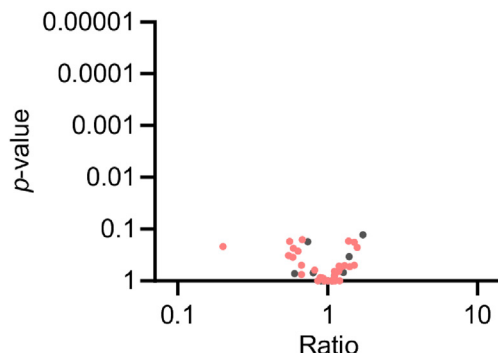
A**B****C**

Figure 5. Connection frequencies are similar in *Orco*^{+/+} and *Orco*^{-/-} flies

(A) A total of 887 and 899 connections between projection neurons and Kenyon cells were mapped in *Orco*^{+/+} and *Orco*^{-/-} female flies that were 2 or 3 days old; all connections are reported in two connectivity matrices (*Orco*^{+/+}, left panel and green; *Orco*^{-/-}, right panel and blue). In each matrix, a row corresponds to a Kenyon cell (250 Kenyon cells per matrix), and each column corresponds to one of the 51 types of projection neuron; each colored bar indicates the input connections of a given Kenyon cell, and the color indicates the number of connections found between a particular Kenyon cell and a given type of projection neuron (blue/green, one connection; red, two connections; black, three connections). The bar graphs above the matrices represent the frequencies at which a particular type of projection neuron connects to Kenyon cells.

(B) The frequencies at which different types of projection neuron connect to Kenyon cells in both datasets is shown (green, *Orco*^{+/+}; blue, *Orco*^{-/-}). Projection neurons are identified based on the glomeruli they innervate: “OR glomeruli” refers to the projection neurons innervating glomeruli that receive input from odorant receptors-expressing neurons; “IR/GR glomeruli” refers to projection neurons innervating glomeruli that receive input from ionotropic receptors/gustatory receptors-expressing neurons. The frequencies of connections measured for a given type of projection neuron in both genotypes are linked with a black line.

(C) The p value measured for each glomerulus was plotted against the ratio of frequencies (ratio = frequency of connections in *Orco*^{-/-}/frequency of connections in *Orco*^{+/+}) measured for each glomerulus (pink, projection neuron(s) receiving input from an OR glomerulus; dark gray, projection neurons receiving input from an IR or GR glomerulus; light gray, unknown).

The statistical significance for each glomerulus was measured using Fischer’s exact test; to control for false positives, p values were adjusted with a false discovery rate using a Benjamini-Hochberg procedure. A ratio of 1 indicates that there is no shift in frequencies between the *Orco*^{+/+} and *Orco*^{-/-} flies, whereas a ratio smaller than 1 indicates that a given type of projection neuron connects more frequently in *Orco*^{-/-}, and a ratio greater than 1 indicates that a given type of projection neuron connects more frequently in *Orco*^{+/+}.

efficiently from the chemosensory environment present in the particular ecological niche of a species. This finding has important ramifications for our understanding of how such fairly subtle,

yet significant connectivity patterns develop and evolve as well as our understanding of how biases in connectivity might be evolutionarily adaptive.

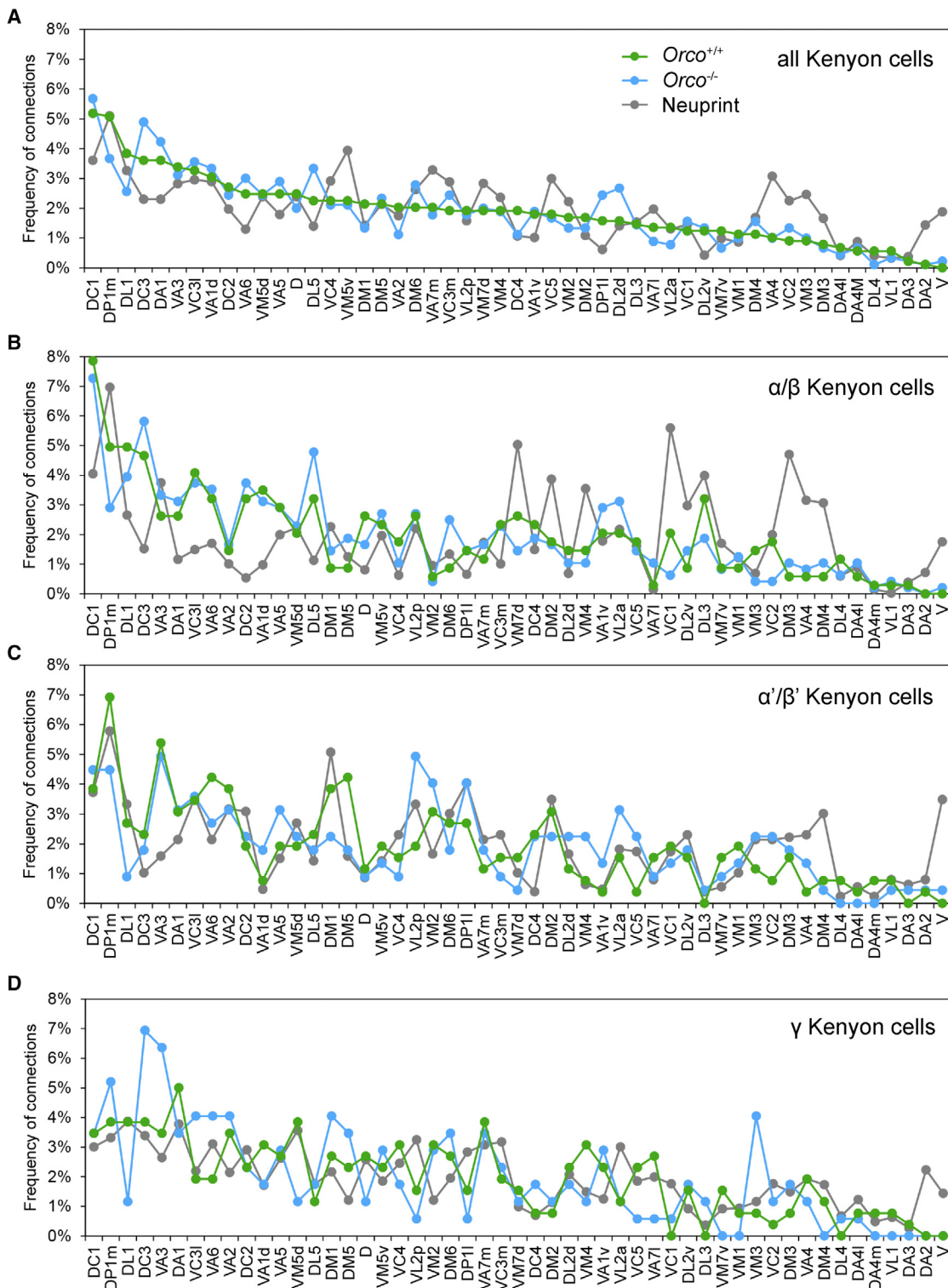


Figure 6. Distributions of connectivity frequencies

The distributions of connectivity frequencies obtained in the experimental datasets—*Orco*^{+/+} (green) and *Orco*^{-/-} (blue)—as well as the connectivity frequencies reported in the hemibrain connectome (gray) were plotted and compared across all Kenyon cells (top), α/β Kenyon cells (middle top), α'/β' Kenyon cells (middle bottom), and γ Kenyon cells (bottom).

The statistical significance for each glomerulus was measured using Fischer's exact test; none of the values were statistically different across the *Orco*^{+/+} and *Orco*^{-/-} datasets ($p < 0.01$). See also Tables S2–S5.

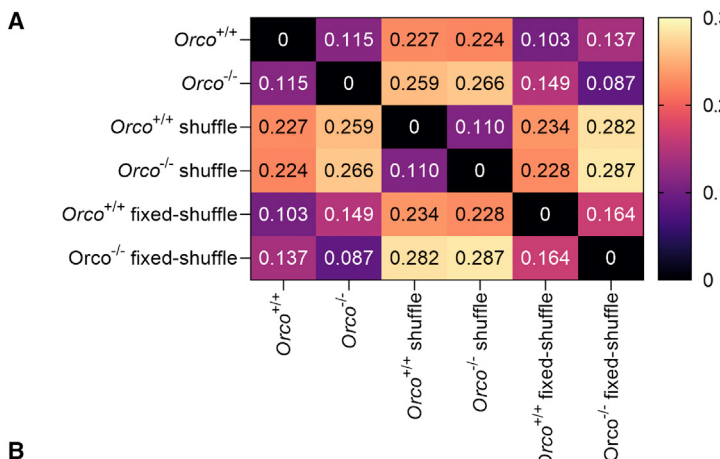
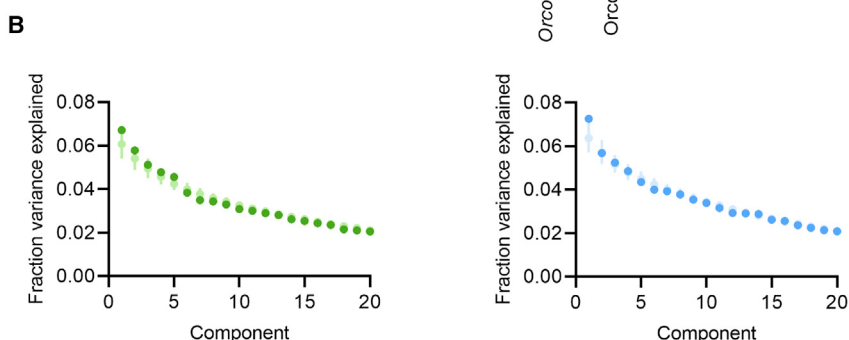


Figure 7. Mushroom body input connectivity is globally similar in *Orco*^{+/+} and *Orco*^{-/-} flies

(A) The Jensen-Shannon distances were measured between the experimental matrices, their shuffle version as well as their fixed-shuffle version. The color bar denotes the range in the distances measured.

(B) Principal components were extracted using either the *Orco*^{+/+} (left panel, green) or the *Orco*^{-/-} (right panel, blue) connectivity matrices—using the experimental and fixed-shuffle versions—and the fraction of the variance explained by each component was measured (dark circles, experimental matrices; light circles, fixed-shuffle versions); error bars represent 95% confidence interval.

See also Figure S4.



STAR★METHODS

Detailed methods are provided in the online version of this paper and include the following:

- **KEY RESOURCES TABLE**
- **RESOURCE AVAILABILITY**
 - Lead contact
 - Materials availability
 - Data and code availability
- **EXPERIMENTAL MODEL AND SUBJECT DETAILS**
 - Fly stocks
- **METHOD DETAILS**
 - Functional imaging
 - Reconstructing antennal lobes
 - Photo-labeling projection neurons and Kenyon cells
 - Mapping Kenyon cell input connections using dye electroporation
 - Quantifying morphological features
- **QUANTIFICATION AND STATISTICAL ANALYSIS**

SUPPLEMENTAL INFORMATION

Supplemental information can be found online at <https://doi.org/10.1016/j.cub.2022.07.055>.

ACKNOWLEDGMENTS

We thank members of the Caron laboratory for comments on the manuscript, Anita Devineni for sharing the code used to analyze imaging data, Cody Orton for the initial characterization of Kenyon cells, Adam Lin for preparation of the standard cornmeal agar medium, Ashley Platt for assistance with general laboratory concerns, María del Carmen Díaz de la Loza for science visualization in

the graphical abstract, and the Cell Imaging Core at the University of Utah for use of the Zeiss LSM 880 microscope. This work has been funded by grants from the National Institute of Neurological Disorders and Stroke (R01 NS 106018, R01 NS 1079790, and R01 EB 029858), the National Science Foundation (IOS 2042397 and DBI 1707398), and the Gatsby Charitable Foundation. Further financial support was provided by the DOE CSGF (DE-SC0022158) (I.G.), the Research Scholar Award (M.S.J.), the University Research Opportunities Program (M.S.J.), the Burroughs Wellcome Fund (A.L.-K.), the McKnight Endowment Fund (A.L.-K.), the Simons Collaboration on the Global Brain (A.L.-K.), and the Georges S. and Dolores Eccles Foundation (S.J.C.C.).

AUTHOR CONTRIBUTIONS

T.T.H. and S.J.C.C. conceived the project. A.J.M. collected and analyzed the calcium imaging data with the help of T.T.H. H.M.S. generated and analyzed the antennal lobe reconstructions. T.T.H. photo-labeled projection neurons and Kenyon cells and analyzed their morphology with the help of M.S.J. T.T.H. and K.E.E. generated the connectivity matrices. I.G. and A.L.-K. performed the statistical analyses of the connectivity matrices. T.T.H. and S.J.C.C. wrote the manuscript with input from all other authors.

DECLARATION OF INTERESTS

The authors declare no competing interests.

Received: November 5, 2021

Revised: May 4, 2022

Accepted: July 21, 2022

Published: August 16, 2022

REFERENCES

- Petrovic, M., and Schmucker, D. (2015). Axonal wiring in neural development: target-independent mechanisms help to establish precision and complexity. *BioEssays* 37, 996–1004.

2. Aso, Y., Hattori, D., Yu, Y., Johnston, R.M., Iyer, N.A., Ngo, T.-T.B., Dionne, H., Abbott, L.F., Axel, R., Tanimoto, H., et al. (2014). The neuronal architecture of the mushroom body provides a logic for associative learning. *eLife* 3, e04577.
3. Li, F., Lindsey, J.W., Marin, E.C., Otto, N., Dreher, M., Dempsey, G., Stark, I., Bates, A.S., Pleijzier, M.W., Schlegel, P., et al. (2020). The connectome of the adult *Drosophila* mushroom body provides insights into function. *eLife* 9, e62576.
4. Couto, A., Alenius, M., and Dickson, B.J. (2005). Molecular, anatomical, and functional organization of the *Drosophila* olfactory system. *Curr. Biol.* 15, 1535–1547.
5. Fishilevich, E., and Vosshall, L.B. (2005). Genetic and functional subdivision of the *Drosophila* antennal lobe. *Curr. Biol.* 15, 1548–1553.
6. Bates, A.S., Schlegel, P., Roberts, R.J.V., Drummond, N., Tamimi, I.F.M., Turnbull, R., Zhao, X., Marin, E.C., Popovici, P.D., Dhawan, S., et al. (2020). Complete connectomic reconstruction of olfactory projection neurons in the fly brain. *Curr. Biol.* 30, 3183–3199.e6.
7. Schlegel, P., Bates, A.S., Stürmer, T., Jagannathan, S.R., Drummond, N., Hsu, J., Serratosa Capdevila, L.S., Javier, A., Marin, E.C., Barth-Maron, A., et al. (2021). Information flow, cell types and stereotypy in a full olfactory connectome. *eLife* 10, e66018.
8. Murthy, M., Fiete, I., and Laurent, G. (2008). Testing odor response stereotypy in the *Drosophila* mushroom body. *Neuron* 59, 1009–1023.
9. Caron, S.J.C., Ruta, V., Abbott, L.F., and Axel, R. (2013). Random convergence of olfactory inputs in the *Drosophila* mushroom body. *Nature* 497, 113–117.
10. Gruntman, E., and Turner, G.C. (2013). Integration of the olfactory code across dendritic claws of single mushroom body neurons. *Nat. Neurosci.* 16, 1821–1829.
11. Litwin-Kumar, A., Harris, K.D., Axel, R., Sompolsky, H., and Abbott, L.F. (2017). Optimal degrees of synaptic connectivity. *Neuron* 93, 1153–1164.e7.
12. Zavitz, D., Amematsro, E.A., Borisuk, A., and Caron, S.J.C. (2021). Connectivity patterns that shape olfactory representation in a mushroom body network model. Preprint at bioRxiv. <https://doi.org/10.1101/2021.02.10.430647>.
13. Kurtovic, A., Widmer, A., and Dickson, B.J. (2007). A single class of olfactory neurons mediates behavioural responses to a *Drosophila* sex pheromone. *Nature* 446, 542–546.
14. Silbering, A.F., Rytz, R., Grosjean, Y., Abuin, L., Ramdy, P., Jefferis, G.S.X.E., and Benton, R. (2011). Complementary function and integrated wiring of the evolutionarily distinct *Drosophila* olfactory subsystems. *J. Neurosci.* 31, 13357–13375.
15. Ebrahim, S.A.M., Dweck, H.K.M., Stökl, J., Hofferberth, J.E., Trona, F., Weniger, K., Rybak, J., Seki, Y., Stensmyr, M.C., Sachse, S., et al. (2015). *Drosophila* avoids parasitoids by sensing their semiochemicals via a dedicated olfactory circuit. *PLoS Biol.* 13, e1002318.
16. Stensmyr, M.C., Dweck, H.K.M., Farhan, A., Ibba, I., Strutz, A., Mukunda, L., Linz, J., Grabe, V., Steck, K., Lavista-Llanos, S., et al. (2012). A conserved dedicated olfactory circuit for detecting harmful microbes in *Drosophila*. *Cell* 151, 1345–1357.
17. Larsson, M.C., Domingos, A.I., Jones, W.D., Chiappe, M.E., Amrein, H., and Vosshall, L.B. (2004). Or83b encodes a broadly expressed odorant receptor essential for *Drosophila* olfaction. *Neuron* 43, 703–714.
18. Benton, R., Sachse, S., Michnick, S.W., and Vosshall, L.B. (2006). Atypical membrane topology and heteromeric function of *Drosophila* odorant receptors *in vivo*. *PLoS Biol.* 4, e20.
19. Task, D., and Potter, C.J. (2021). Rapid degeneration of *Drosophila* olfactory neurons in Orco mutant maxillary palps. MicroPublication Biol. <https://doi.org/10.17912/micropub.biology.000398>.
20. Chiang, A., Priya, R., Ramaswami, M., Vijayraghavan, K., and Rodrigues, V. (2009). Neuronal activity and Wnt signaling act through GSK3-β to regulate axonal integrity in mature *Drosophila* olfactory sensory neurons. *Development* 136, 1273–1282.
21. Jones, W.D., Cayirlioglu, P., Kadow, I.G., and Vosshall, L.B. (2007). Two chemosensory receptors together mediate carbon dioxide detection in *Drosophila*. *Nature* 445, 86–90.
22. Kwon, E.Z., Kazmar, T., Stampfel, G., Yáñez-Cuna, J.O., Pagani, M., Schernhuber, K., Dickson, B.J., and Stark, A. (2014). Genome-scale functional characterization of *Drosophila* developmental enhancers *in vivo*. *Nature* 512, 91–95.
23. Ronderos, D.S., Lin, C.-C., Potter, C.J., and Smith, D.P. (2014). Farnesol-detecting olfactory neurons in *Drosophila*. *J. Neurosci.* 34, 3959–3968.
24. Olsen, S.R., Bhandawat, V., and Wilson, R.I. (2007). Excitatory interactions between olfactory processing channels in the *Drosophila* antennal lobe. *Neuron* 54, 89–103.
25. Neuhaus, E.M., Gisselmann, G., Zhang, W., Dooley, R., Störtkuhl, K., and Hatt, H. (2005). Odorant receptor heterodimerization in the olfactory system of *Drosophila melanogaster*. *Nat. Neurosci.* 8, 15–17.
26. Kazama, H., Yaksi, E., and Wilson, R.I. (2011). Cell death triggers olfactory circuit plasticity via glial signaling in *Drosophila*. *J. Neurosci.* 31, 7619–7630.
27. Berdnik, D., Chihara, T., Couto, A., and Luo, L. (2006). Wiring stability of the adult *Drosophila* olfactory circuit after lesion. *J. Neurosci.* 26, 3367–3376.
28. Trible, W., Olivos-Cisneros, L., McKenzie, S.K., Saragosti, J., Chang, N.-C., Matthews, B.J., Oxley, P.R., and Kronauer, D.J.C. (2017). Orco mutagenesis causes loss of antennal lobe glomeruli and impaired social behavior in ants. *Cell* 170, 727–735.e10.
29. Ryba, A.R., McKenzie, S.K., Olivos-Cisneros, L., Clowney, E.J., Pires, P.M., and Kronauer, D.J.C. (2020). Comparative development of the ant chemosensory system. *Curr. Biol.* 30, 3223–3230.e4.
30. Scheffer, L.K., Xu, C.S., Januszewski, M., Lu, Z., Takemura, S.Y., Hayworth, K.J., Huang, G.B., Shinomiya, K., Maitlin-Shepard, J., Berg, S., et al. (2020). A connectome and analysis of the adult *Drosophila* central brain. *eLife* 9, e57443.
31. Devaud, J.-M., Acebes, A., and Ferrús, A. (2001). Odor exposure causes central adaptation and morphological changes in selected olfactory glomeruli in *Drosophila*. *J. Neurosci.* 21, 6274–6282.
32. Devaud, J.-M., Acebes, A., Ramaswami, M., and Ferrús, A. (2003). Structural and functional changes in the olfactory pathway of adult *Drosophila* take place at a critical age. *J. Neurobiol.* 56, 13–23.
33. Sachse, S., Rueckert, E., Keller, A., Okada, R., Tanaka, N.K., Ito, K., and Vosshall, L.B. (2007). Activity-dependent plasticity in an olfactory circuit. *Neuron* 56, 838–850.
34. Mayseless, O., Rachad, E.Y., Shapira, G., Fiala, A., and Schuldiner, O. (2021). Silencing neuronal activity is required for developmental circuit remodeling. Preprint at bioRxiv. <https://doi.org/10.1101/2021.10.31.466652>.
35. Zheng, Z., Li, F., Fisher, C., Ali, I.J., Sharifi, N., Calle-Schuler, S., Hsu, J., Masoodpanah, N., Kmecova, L., Kazimiers, T., et al. (2020). Structured sampling of olfactory input by the fly mushroom body. Preprint at bioRxiv. <https://doi.org/10.1101/2020.04.17.047167>.
36. Kremer, M.C., Christiansen, F., Leiss, F., Paehler, M., Knapek, S., Andlauer, T.F.M., Förstner, F., Kloppenburg, P., Sigrist, S.J., and Tavosanis, G. (2010). Structural long-term changes at mushroom body input synapses. *Curr. Biol.* 20, 1938–1944.
37. Doll, C.A., Vita, D.J., and Broadie, K. (2017). Fragile X mental retardation protein requirements in activity-dependent critical period neural circuit refinement. *Curr. Biol.* 27, 2318–2330.e3.
38. Pech, U., Revelo, N.H., Seitz, K.J., Rizzoli, S.O., and Fiala, A. (2015). Optical dissection of experience-dependent pre- and postsynaptic plasticity in the *Drosophila* brain. *Cell Rep.* 10, 2083–2095.
39. Baltruschat, L., Prisco, L., Ranft, P., Lauritzen, J.S., Fiala, A., Bock, D.D., and Tavosanis, G. (2021). Circuit reorganization in the *Drosophila* mushroom body calyx accompanies memory consolidation. *Cell Rep.* 34, 108871.

40. Sugie, A., Marchetti, G., and Tavosanis, G. (2018). Structural aspects of plasticity in the nervous system of *Drosophila*. *Neural Dev.* **13**, 14.
41. Elkahlah, N.A., Rogow, J.A., Ahmed, M., and Clowney, E.J. (2020). Presynaptic developmental plasticity allows robust sparse wiring of the *Drosophila* mushroom body. *eLife* **9**, e52278.
42. Devineni, A.V., Sun, B., Zhukovskaya, A., and Axel, R. (2019). Acetic acid activates distinct taste pathways in *Drosophila* to elicit opposing, state-dependent feeding responses. *eLife* **8**, e47677.
43. Schindelin, J., Arganda-Carreras, I., Frise, E., Kaynig, V., Longair, M., Pietzsch, T., Preibisch, S., Rueden, C., Saalfeld, S., Schmid, B., et al. (2012). Fiji: an open-source platform for biological-image analysis. *Nat. Methods* **9**, 676–682.
44. Wan, Y., Otsuna, H., Chien, C.-B., and Hansen, C. (2012). FluoRender: an application of 2D image space methods for 3D and 4D confocal microscopy data visualization in neurobiology research. *IEEE Pac. Vis. Symp.* 201–208.
45. Longair, M.H., Baker, D.A., and Armstrong, J.D. (2011). Simple Neurite Tracer: open source software for reconstruction, visualization and analysis of neuronal processes. *Bioinformatics* **27**, 2453–2454.
46. Hattori, D., Aso, Y., Swartz, K.J., Rubin, G.M., Abbott, L.F., and Axel, R. (2017). Representations of novelty and familiarity in a mushroom body compartment. *Cell* **169**, 956–969.e17.
47. Devineni, A.V., Deere, J.U., Sun, B., and Axel, R. (2021). Individual bitter-sensing neurons in *Drosophila* exhibit both ON and OFF responses that influence synaptic plasticity. *Curr. Biol.* **31**, 5533–5546.e7.
48. Guizar-Sicairos, M., Thurman, S.T., and Fienup, J.R. (2008). Efficient sub-pixel image registration algorithms. *Opt. Lett.* **33**, 156–158.
49. Grabe, V., Strutz, A., Baschwitz, A., Hansson, B.S., and Sachse, S. (2015). Digital *in vivo* 3D atlas of the antennal lobe of *Drosophila melanogaster*. *J. Comp. Neurol.* **523**, 530–544.
50. Li, J., Ellis, K.E., and Caron, S.J.C. (2021). Photo-labeling neurons in the *Drosophila* brain. *Star Protoc.* **2**, 100381.
51. Wan, Y., Otsuna, H., Holman, H.A., Bagley, B., Ito, M., Lewis, A.K., Colasanto, M., Kardon, G., Ito, K., and Hansen, C. (2017). FluoRender: joint freehand segmentation and visualization for many-channel fluorescence data analysis. *BMC Bioinformatics* **18**, 280.

STAR★METHODS

KEY RESOURCES TABLE

REAGENT or RESOURCE	SOURCE	IDENTIFIER
Antibodies		
Mouse monoclonal anti-nc82	Developmental Studies Hybridoma Bank	RRID: AB_2314866
Goat anti-Mouse IgM (Heavy chain) Cross-Adsorbed Secondary Antibody, Alexa Fluor 488	Thermo Fisher Scientific	Cat# A-21042; RRID: AB_2535711
Chemicals, peptides, and recombinant proteins		
normal goat serum	The Jackson Laboratory	RRID: AB_2336990
VECTASHIELD mounting medium	Vector Laboratories	Cat#H-1000
16% paraformaldehyde	Electron Microscopy Sciences	Cat#15710
10X phosphate buffered saline	Sigma-Aldrich	Cat#P5493
TexasRed dye	Thermo-Fisher	Cat#D3328
Triton X-100	Sigma-Aldrich	Cat#T8787
Collagenase	Sigma-Aldrich	Cat#C5138
MgCl ₂ solution (1M in H ₂ O)	Sigma-Aldrich	Cat#63069
CaCl ₂ solution (1M in H ₂ O)	Sigma-Aldrich	Cat#21115
NaOH solution (10M in H ₂ O)	Sigma-Aldrich	Cat#72068
NaCl	Sigma-Aldrich	Cat#S7653
KCl	Sigma-Aldrich	Cat#P5405
HEPES	Sigma-Aldrich	Cat#H3375
Trehalose	Sigma-Aldrich	Cat#T0167
Sucrose	Sigma-Aldrich	Cat#S1888
NaHCO ₃	Sigma-Aldrich	Cat#S5761
NaH ₂ PO ₄	Sigma-Aldrich	Cat#S5011
Isopentyl acetate	Sigma-Aldrich	Cat#112674
1-pentanol	Sigma-Aldrich	Cat#77597
3-octanol	Sigma-Aldrich	Cat#218405
Geranyl acetate	Sigma-Aldrich	Cat#173495
Methyl salicylate	Sigma-Aldrich	Cat#M2047
Paraffin oil	Fluka Analytical	Cat#76235
Acetic acid, glacial	Fisher Scientific	Cat#A38S
Deposited data		
Raw data	This paper	https://github.com/ishanigan/hayashi-et-al-2022
Analyzed connectivity matrices	This paper	https://github.com/ishanigan/hayashi-et-al-2022
Experimental models: Organisms/strains		
<i>D. melanogaster</i> : w ¹¹¹⁸ ;;	Bloomington Drosophila Stock Center	BDSC: 5905
<i>D. melanogaster</i> : w ¹¹¹⁸ ;13XLexAop2-IVS-GCaMP6f-p10 ^{su(Hw)attP5} ;;	Bloomington Drosophila Stock Center	BDSC: 44277
<i>D. melanogaster</i> : w ¹¹¹⁸ ; GMR13F02-lexA ^{attP40} /CyO;;	Bloomington Drosophila Stock Center	BDSC: 52460
<i>D. melanogaster</i> : w*;Orco ² ;	Bloomington Drosophila Stock Center	BDSC: 23130
<i>D. melanogaster</i> : yw;N-Synaptobrevin-GAL4 ^{2.1} ;;	Simpson Lab	N/A

(Continued on next page)

Continued

REAGENT or RESOURCE	SOURCE	IDENTIFIER
<i>D. melanogaster</i> : <i>yw;10xUAS-IVS-Syn21-mC3PA-GFP-p10^{attP40};;</i>	Aso et al. ²	N/A
Software and algorithms		
Code to analyze connectivity matrices	This paper	https://github.com/ishanigan/hayashi-et-al-2022
Code to analyze Ca ²⁺ imaging data	Devineni et al. ⁴²	N/A
FIJI	Schindelin et al., 2012 ⁴³	https://imagej.nih.gov/ij/
Fluorender version 2.26.2	Wan et al. ⁴⁴	https://github.com/SCInstitute/fluorender/
MATLAB	Mathworks	https://www.mathworks.com/products/matlab.html
Simple Neurite Tracer	Longair et al. ⁴⁵	https://imagej.net/plugins/simple-neurite-tracer
ZEN microscope software	Zeiss	RRID: SCR_013672
Amira version 2020.3.1	Thermo Fisher Scientific	RRID: SCR_007353
Other		
Dumont #55 forceps	Fine Science Tools	Cat#11295-51
Clear tape	Shurtape Technologies	Cat#DUC280068
Environmental Chamber	Percival Scientific	Cat#DR36VLC8
Fisherbrand Premium Cover Glasses	Fisher Scientific	Cat#12548A
Fisherbrand Superfrost Disposable Microscope Slides	Fisher Scientific	Cat#12-550-143
GaAsP detector	Hamamatsu Photonics	N/A
PMT detector	Bruker	N/A
Borosilicate glass pipette with filaments	Sutter Instrument	Cat#BF100-50-10
Micro-forge	Narishige	Cat#MF-900
Micromanipulator	Sutter Instrument	Cat#MP-265
Polystyrene Petri-dish 35 mm × 10 mm	Thermo Fisher Scientific	Cat#FB0875711YZ
Stimulus controller	Ockenfels Syntech	Cat#CS-55
SYLGARD 184	Electron Microscopy Sciences	Cat#24236-10
Tungsten 99.95% CS	California Fine Wire Company	Cat#100211
Objective C Plan-Apochromat 63x/1.4 Oil DIC M27	Zeiss	Cat#421782-9900-799
P-2000 Laser Micropipette Puller	Sutter Instrument	RRID: SCR_018640
Pockel cells	Conoptics	Cat#350-80LA/BK-02
Ultrafast Chameleon Ti:sapphire laser	Coherent	N/A
UV glue	Bondic	Cat#SK8024
Bruker Ultima investigator multiphoton microscope	Bruker	RRID: SCR_019807
Water Immersion Lens 60x	Olympus	Cat#N2667800
Zeiss LSM 880 with Airyscan Confocal Laser Scanning Microscope	Zeiss	RRID: SCR_020925

RESOURCE AVAILABILITY**Lead contact**

Requests for information and resources should be directed to and will be fulfilled by the lead contact, Sophie J.C. Caron (sophie.caron@utah.edu).

Materials availability

This research did not produce new unique reagents.

Data and code availability

All raw data, the connectivity matrices and the code used to analyze these matrices are available on <https://github.com/ishanigan/hayashi-et-al-2022>. Any additional information required to reanalyze the data reported in this paper is available from the lead contact.

EXPERIMENTAL MODEL AND SUBJECT DETAILS**Fly stocks**

Flies (*Drosophila melanogaster*) were fed on standard cornmeal agar medium and raised in a controlled environmental chamber (Percival Scientific, Cat#DR36VL) that maintains a temperature of 25°C and 60% humidity under a 12 hours/12 hours light-dark cycle. Crosses were set up and reared under the same conditions, but the standard cornmeal agar medium was supplemented with dry yeast. Two- or three-day-old female flies were used in all experiments. For the functional imaging experiments, we used the following transgenic lines: *w; [GMR13F02-LexA]^{attP40}, [13xLexAop2-IVS-GCaMP6f-p10]^{su(Hw)attP5}/+;*; (referred to in the text as 'Orco^{+/+}') and *w; [GMR13F02-LexA]^{attP40}, [13xLexAop2-IVS-GCaMP6f-p10]^{su(Hw)attP5}/+;Orco²*; (referred to in the text as 'Orco^{-/-}'). For the antennal lobe reconstructions, we used the following transgenic lines: *w;+;+;+, (referred to in the text as 'Orco^{+/+}) w;+;Orco²;+ (referred to in the text as 'Orco^{-/-}')*. For the photolabeling and connectivity mapping experiments, we used the following transgenic lines: *w;[N-Synaptobrevin-GAL4]^{2.1}, [10xUAS-IVS-Syn21-mC3PA-GFP-p10]^{attP40};*; (referred to in the text as 'Orco^{+/+}') and *w;[N-Synaptobrevin-GAL4]^{2.1}, [10xUAS-IVS-Syn21-mC3PA-GFP-p10]^{attP40};Orco²*; (referred to in the text as 'Orco^{-/-}'). All Orco^{-/-} lines were genotyped every other month by performing PCR using a previously established protocol.¹⁷

METHOD DETAILS**Functional imaging**

Calcium imaging experiments were performed on immobilized flies. Flies were immobilized underneath an imaging chamber — a platform with an opening attached to a reservoir of saline — using a combination of clear tape (Shurtape Technologies, Cat#DUC280068) and UV glue (Bondic, Cat#SK8024). A hole was cut in the head cuticle of the fly, above the mushroom body, and the exposed brain was submerged in saline (108 mM NaCl, 5 mM KCl, 5 mM HEPES, 5 mM Trehalose, 10 mM Sucrose, 1 mM NaH₂PO₄, 4 mM NaHCO₃, 2 mM CaCl₂, 4 mM MgCl₂, 1.7 mM NaOH, pH ≈ 7.3). Immobilized flies were exposed to an odor — either isopentyl acetate (Sigma-Aldrich, Cat#112674), 1-pentanol (Sigma-Aldrich, Cat#77597), 3-octanol (Sigma-Aldrich, Cat#218405), geranyl acetate (Sigma-Aldrich, Cat#173495), methyl salicylate (Sigma-Aldrich, Cat#M2047) diluted 5% volume to volume in paraffin oil (Fluka Analytical, Cat#76235) or acetic acid (Fisher Scientific, Cat#A38S) diluted 5% volume to volume in water — using a stimulus controller (Ockenfels Syntech GmbH, Cat#CS-55). Calcium transients were measured using an Investigator two-photon laser scanning microscope (Bruker Corporation, RRID: SCR_019807) equipped with an ultrafast Chameleon Ti:Sapphire laser (Coherent) modulated by Pockels Cells (Conoptics, Cat#350-80LA/BK-02). The laser power used for each experiment varied from 14 to 24 mW. Calcium transients were recorded in the calyx of the mushroom body using the following sequence: five seconds odor 'off', two seconds odor 'on', eight seconds odor 'off', two seconds odor 'on', and eight seconds odor 'off'. This sequence was repeated four times. Image sequences were collected with either a galvo and 512 by 512 pixels resolution with 0.8 μs dwell time and 1.64 fps (for generating the data shown in Figures 1A, 1C, S1A, and S1C) or a resonant galvo and 512 by 512 resolution with 15.081 fps (for generating the data shown in Figures 1B and S1B). Calcium transients were analyzed using a custom MATLAB (MathWorks) code based on previously published codes.^{42,46,47} To correct for movement, images were registered within and between trials using a sub-pixel registration algorithm.⁴⁸ Heatmaps were generated by averaging the intensity of individual pixels (F₀: The entire five seconds of the first off-period combined with the last two seconds of the second off-period; F: The entire two seconds of the on-period). Traces were generated by averaging the calcium transients detected in the main calyx (F₀: The entire five seconds of the first off-period combined with the last two seconds of the second off-period; F: The entire two seconds of the on-period).

Reconstructing antennal lobes

Antennal lobes were reconstructed from confocal images of fixed brains based on a protocol developed by previous studies.^{48,49} In summary, the brains of flies were dissected using Dumont #55 forceps (Fine Science Tools (USA), Cat#11295-51) at room temperature in a phosphate buffered saline solution or PBS (Sigma-Aldrich, Cat#P5493), fixed in 2% paraformaldehyde (Electron Microscopy Sciences, Cat#15710) for 45 minutes at room temperature, washed five times in PBST (PBS supplemented with 0.1% Triton X-100, Sigma-Aldrich, Cat#T8787) at room temperature, blocked with 5% goat Serum (Jackson ImmunoResearch Laboratories, RRID: AB_2336990) in PBST for 30 minutes at room temperature, and incubated in a solution that contained the primary antibody (1:20 in 5% Goat Serum/PBST, Developmental Studies Hybridoma Bank, nc82, RRID: AB_2314866) at 4°C overnight. On the following day, brains were washed four times in PBST and incubated in a solution that contained the secondary antibody (1:500 in 5% Goat Serum/PBST, Thermal Fisher, goat anti-mouse Alexa Fluor 488, RRID: AB_2576217) at 4°C overnight. On the following day, brains were washed four times in PBST and mounted on a slide (Fisher Scientific, Cat#12-550-143) using the mounting medium VECTASHIELD (Vector Laboratories, Cat#H-1000) and cover glasses (Fisher Scientific, Cat#12548A). Immuno-stained brains were imaged using a Zeiss LSM 880 with Airyscan Confocal Laser Scanning Microscope (RRID: SCR_020925) equipped with a 63X oil immersion objective. Images were captured at a frame size of 1056 pixels by 1056 pixels (pixel size: 0.106 μm) and a digital zoom of 1.2 using the ZEN microscope software (Carl Zeiss AG, RRID: SCR_013672). Sections were taken at 1 μm interval and each antennal lobe could be imaged with a minimum of 45 and a maximum of 63 sections. Antennal lobes were reconstructed from these images using the segmentation software Amira (Thermo Fisher Scientific, Amira version 2020.3.1, RRID: SCR_007353). Individual glomeruli were defined by manually identifying regions of interest for each glomerulus in the 'Segmentation' tab; the 'Interpolate' and 'Generate Surface' functions were used to generate the reconstructions. The volumes of the reconstructed glomeruli were

extracted by using the 'Material Statistics' function which scales the objects to μm units based on the voxel size ($0.0113 \mu\text{m}^3$ as estimated by ImageJ). Glomeruli were assigned identities according to their position based on the available anatomical maps and the *Drosophila melanogaster* hemibrain connectome v1.2.1.^{4,5,30,49} Glomerular volumes were calculated from the reconstructed voxel size, and the sum of those volumes were used to calculate whole antennal lobe volumes. A total of ten antennal lobes — five *Orco*^{+/+} and five *Orco*^{-/-} antennal lobes — were reconstructed.

Photo-labeling projection neurons and Kenyon cells

Neurons were photo-labeled based on a previously published protocol. In short, brains were dissected in saline, treated for one minute with 2 mg/ml collagenase (Sigma-Aldrich, Cat#C5138) and mounted on a piece of Sylgard (Electron Microscopy Sciences, Cat#24236-10) placed at the bottom of a Petri dish (Thermo Fisher Scientific, Cat#FB0875711YZ). Each brain was mounted using pins of Tungsten 99.95% CS (California Fine Wire Company, Cat#100211), either with its anterior side facing upward (for photo-labeling projection neurons) or with its posterior side facing upward (for photo-labeling Kenyon cells). The photo-labeling and image acquisition steps were performed using an Ultima two-photon laser scanning microscope (Bruker Corporation, RRID: SCR_019807) with an ultrafast Chameleon Ti:Sapphire laser (Coherent) modulated by Pockels Cells (Conoptics, Cat#350-80LA/BK-02). During the photo-labeling step, the laser was tuned to 710 nm and about 5 to 30 mW of laser power was used; during the image acquisition step, the laser was tuned to 925 nm and about 1 to 14 mW of laser power was used. Both power values were measured behind the objective lens. A 60X water-immersion objective lens (Olympus Corporation, Cat#N2667800) was used for both photo-labeling and image acquisition. A GaAsP detector (Hamamatsu Photonics K.K.) and PMT detector (Bruker Corporation) were used for measuring green and red fluorescence, respectively. Photo-labeling was performed by drawing a region of interest — on average $1.0 \times 1.0 \mu\text{m}$ — either in the center of the targeted glomerulus (for labeling projection neurons) or in the center of the soma (for labeling Kenyon cells); each pixel was scanned 8 times. Image acquisition was performed at a resolution of 512 by 512 pixels with a pixel size of $0.39 \mu\text{m}$ and a pixel dwell time of 4 μs ; each pixel was scanned 2 times. A minimum of eight samples were analyzed for each type of projection neuron in a given genotype.

Mapping Kenyon cell input connections using dye electroporation

The projection neurons connecting to a photo-labeled Kenyon cell were identified as described before with some modification.⁹ In short, electrodes were made by pulling borosilicate glass pipette with filament (Sutter Instrument, Cat#BF100-50-10) to a resistance of 9-11 M Ω , fire-polished using a micro-forge (Narishige International USA) to narrow their opening, and backfilled with 100mg/ml 3000-Da Texas-dextran dye (Thermo-Fisher Scientific, Cat#D3328). Under the guidance of an Ultima two-photon microscope (Bruker Corporation, RRID: SCR_019807), an electrode was centered into the postsynaptic terminal — or 'claw' — of a photo-labeled Kenyon cell using a motorized micromanipulator (Sutter Instrument, Cat#MP-265). Short current pulses (each 10-50 V in amplitude and 0.5 millisecond long) were applied until the projection neuron connecting to the targeted Kenyon cell claw was visible. An image of the antennal lobe was acquired at the end of the procedure. Dye-labeled glomeruli were identified based on their shape, position and the location of their soma as defined in the available anatomical maps and the *Drosophila melanogaster* hemibrain connectome v1.2.1.^{4,5,30,49} The inputs of 200 randomly-selected Kenyon cells were mapped using this protocol. To increase the number of α'/β' Kenyon cells in each data set, α'/β' Kenyon cells were pre-selected by weakly photo-labeling a region of the α'/β' mushroom body lobe using a published protocol.⁵⁰ Not all the projection neurons connecting to a given Kenyon cells in a given experiment could be dye-filled but on average 4 ± 1 (mean \pm standard deviation) of the claws formed by a given Kenyon cell were dye-filled. Frequencies of connections were calculated as the sampled number of connections from a given glomerulus divided by the total number of sampled connections. Frequencies of connections for Neuprint hemibrain connectome v1.2.1 was calculated from the number of synaptic active zones from a given projection neuron type to Kenyon cells.³⁰ Our dataset defines a connection based on the bouton-claw pair, while Neuprint is based on synaptic active zones.

Quantifying morphological features

All quantifications were done blindly without prior knowledge of the genotype of a sample. Representative images of antennal lobes, projection neurons, Kenyon cells were projected at maximal intensity using the ImageJ/Fiji software (National Institutes of Health⁴³). Projection neurons were counted based on the number of photo-labeled bodies observed in the anterior or lateral clusters of the antennal lobe. Primary branches were defined as processes that emerge from the main axonal projection traversing the calyx of the mushroom body. The length of the branches formed by a neuron (projection neuron or Kenyon cell) and the lengths of the claws formed by a Kenyon cell was quantified using the 'Simple Neurite Tracer' plugin and the ImageJ/Fiji software (National Institutes of Health^{45,43}). Simple Neurite Tracer allows to manually trace the continuous neurite processes found in the image across a Z-stack. When measuring the total and average branch length of a Kenyon cell, the main track — defined as the neurite that emerges from the soma and traverses the peduncle — was excluded and only the branches emerging from the main track were traced. Claws were defined as cup-like endings located at the end of a dendritic process formed by a Kenyon cell. When measuring claw length, the perimeter of the cup-like structure was traced. The length of a given trace was measured using the 'Measure' and 'Cable Length' functions. The total bouton volume was measured using Fluorender (University of Utah Scientific Computing and Imaging Institute; version 2.26.2^{44,51}): boutons were traced using the 'Paint Brush' function. To efficiently distinguish boutons from the background, the 'Edge Detect' parameter was kept on and the 'Edge STR' was fixed at 0.505, while the selection threshold was adjusted to different values depending on signal intensity. The 'Physical Size' value was reported as total bouton volume.

QUANTIFICATION AND STATISTICAL ANALYSIS

For the statistical analyses of the data shown in [Figures 1, 2, 3, 4, S1](#), and [S2](#), p values were computed using the Mann-Whitney U test; statistical significance is indicated as $p < 0.05$ (*), $p < 0.01$ (**) and $p < 0.001$ (***)³⁵. For the statistical analyses of the data shown in [Figures 5C](#) and [6](#) and [Tables S2–S5](#), p values were computed using the Fisher's exact test; to control for false positives, p values were adjusted with a false discovery rate of 10% using a Benjamini-Hochberg procedure. The methods used to generate the conditional input matrices shown in [Figure S4](#) have been described in a previous study.³⁵ In short, each cell in the conditional input matrices indicates whether a Kenyon cell is more, equally or less likely than chance to receive an input from a type of projection neuron (column) given that this Kenyon cell receives an input from another type of projection neuron (row). Each observed projection neuron-Kenyon cell connection is treated as a single count. The observed number of counts for a given pair of neurons is compared to the distribution of counts generated using a null model. In the null model, 1,000 connectivity matrices were generated by randomly shuffling the connections recorded in the corresponding experimental matrix while keeping the number of input each Kenyon cell receives and the frequencies at which projection neurons connect to Kenyon cells constant; these matrices are referred in the main text as 'fixed shuffle matrices'. For each pair of projection neurons, a z-score representing the number of standard deviations from the mean of the null distribution and the observed counts was computed.